Hindawi
International Journal of Antennas and Propagation
Volume 2023, Article ID 8825446, 13 pages
https://doi.org/10.1155/2023/8825446

Research Article

On the Experimental Investigation of Bone Fracture Recovery Process Using an Ultra-Wideband Planar Monopole Antenna

Shaik Rizwan, Kanaparthi V. Phani Kumar, and Sandeep Kumar Palaniswamy

Diagnostics, Therapeutics and Assistive Devices Laboratory, Department of Electronics and Communication Engineering, Faculty of Engineering and Technology, SRM Institute of Science and Technology, Kattankulathur, Tamil Nadu 603203, India

Correspondence should be addressed to Kanaparthi V. Phani Kumar; kvphanikumar264@gmail.com

Received 10 April 2023; Revised 23 May 2023; Accepted 14 July 2023; Published 26 July 2023

Academic Editor: Rajkishor Kumar

In this paper, a noninvasive bone fracture monitoring system is developed using a planar monopole antenna. The proposed antenna provides an ultra-wideband response, and its overall size is $18 \times 19 \times 0.8\ mm^3$. The proposed ultra-wideband monopole (UWM) antenna has a maximum measured gain of 3.77 dBi, and the maximum SAR value for an input power of 18 dBm is less than 1.6 (W/kg) (1 g). A bovine tibia is experimentally tested using a proposed UWM antenna to monitor the fracture recovery process and then further analysed using principle component and linear regression analysis. In addition, a microcontroller with a wireless communication module is developed to monitor the data in an Android application. The proposed system could be a promising approach for developing a portable, noninvasive monitoring device.

1. Introduction

Human bones are divided into five categories based on their basic morphologies and endochondral or membranous characteristics. These categories are as follows: long, short, flat, sesamoid, and irregular [1]. The tibia is a shaft connected to two ends of the epiphysis. It is the longest bone and is situated at the bottom end of the leg. Most of the time, children, athletes, and older people who do not get enough vitamins, have weak bones, or get into accidents can break their tibia [2]. Hence, the breaks in the bones are classified into different categories. If the bone ends pierce the skin, the fracture is classified as a laceration. If it is a complete break, the break is classified as a sprain and an orientation break [3]. Normal healing of a bone fracture involves the formation of a blood clot and callus to shield the injured area. New strands of bone cells sprout on both sides of the fracture. The connections between these strands are strengthening. When the bone has fully healed, the callus will fall off. Figure 1 depicts the stages of fracture healing. In general, it takes 6–8 weeks for a fracture to heal. However, this time frame is highly variable, both between bones and between individuals. In contrast to a tibia fracture, which can take up to 20 weeks to heal, hand and wrist fractures often mend in only 4–6 weeks [4]. Monitoring the blood clots in a fracture area can assist us in estimating the rate of recovery.

Currently, there are no standardized procedures for monitoring fracture healing; physicians rely on X-rays, which are only useful in the later phases of fracture recovery. X-rays and other conventional diagnosis techniques such as computed tomography (CT), magnetic resonance imaging (MRI), and positron emission tomography (PET) scans are used to monitor the area around soft tissue to find different types of bone fractures [5]. These techniques use high levels of ionised radiation to monitor the bone fractures in the human body [6]. According to the World Health Organization (WHO), the continuous radiation exposure to the human body may cause cancer [7].

Several researchers have proposed various methods for monitoring at lower and higher frequencies, such as a compact microwave device developed for fracture diagnosis [8]. This method uses the Lanczos imaging technique to visualize the fracture by using the transmission characteristics of a microwave ring resonator. The reported sensor operated at 2.45 GHz and losing the high-frequency contents during image restoration results in blurring in the

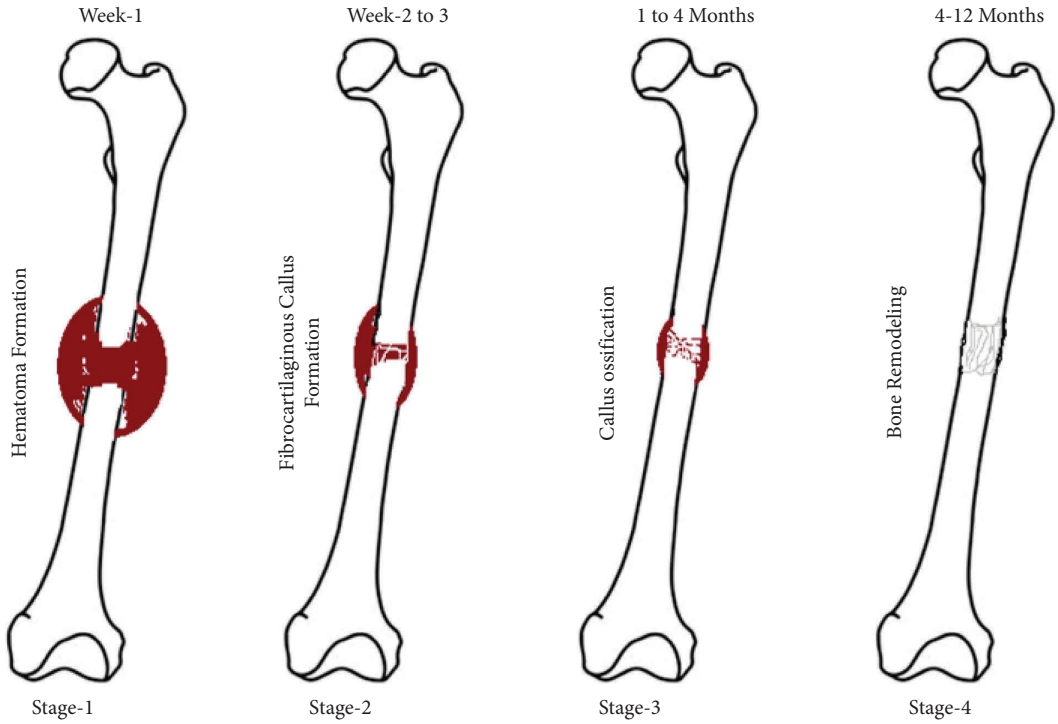

Figure 1: The stages of healing of bone fracture.

image. A UWB textile antenna operating in the range of 1.198–4.055 GHz is reported in [9] for various biomedical applications. The proposed antenna is not low-profile, and there is no adequate detection system to reconstruct the image and monitor the body's subcutaneous interior damage.

In [10], a planar monopole antenna was developed to detect bone cracks or voids. The developed system is used to detect bone cracks or voids based on a shift in the resonance frequency of the reported antenna. It would be difficult to incorporate this antenna into a portable microwave system because of its large size. A smart bone plate for monitoring fracture healing was developed [11], and electrical impedance spectroscopy was employed to monitor the healing tissue. The impedance of the bone plates can be examined by sending current into them and measuring the change in impedance to monitor the stage of fracture healing. However, the reported system depends on the impedance variation. If the impedance is minimal, then differentiation between them is a difficult task [12–16].

In [17], a meta-material-based antenna array is designed for the identification of cancerous cells in biological tissue. The modelled antenna array operated over a 2–12 GHz range. In this method, a realistic phantom breast model is developed, and the model is surrounded by an antenna array, which sends the signal using a single antenna and receives it using the remaining antennas. The magnitude and phase of received signals are recorded to differentiate healthy and unhealthy tissue by dielectric characterization. A UWB antenna operating in a 3 to 15 GHz band is used to investigate the specific absorption rate (SAR) for breast cancer detection, as reported in [18]. Here, the detection of abnormalities was carried out based on simulated SAR values and was not validated experimentally.

In microwave sensing [19], an antenna is used to transmit a radio-frequency signal to tissues. As a result of the higher dielectric constant of unhealthy tissue, the received signals are dispersed differently. The tumor is also identified by dielectric characterization as both healthy and malignant tissue. Therefore, there is space to develop effective antennas with a robust detecting system for a wide range of biomedical applications such as for the wireless body area networks (WBANs) and wearable devices: The planar monopole antennas used in wearable devices or WBANs typically require moderate gain [20]. The planar monopole antenna could be used to detect abnormalities in the human body because it is easy to develop and fabricate on a dielectric substrate and easy to integrate with other devices [20–24].

In this work, a new approach for monitoring the recovery process of bone fractures is proposed using an ultra-wideband monopole (UWM) antenna and data processing techniques. Here, machine learning preprocessing techniques are used for monitoring the recovery process and detecting the length of the blood clots to estimate the recovery rate. One is principal component analysis (PCA), and the other is linear regression analysis (LRA). PCA is used to determine whether the bone is fractured or not, and LRA is used to detect the length of the blood clot. Using PCA, the data can be explored easily to determine the most critical variables and where potential outliers could be hidden [25]. The statistical technique known as regression analysis is used

to investigate the nature of the connection that exists between two different variables. These two methods are used to analyse the data which are received from the antenna.

2. The UWM Antenna Geometry

The evolution of the UWM antenna is shown in Figure 2. The structure of the proposed UWM antenna is composed of three layers. The front and back layers are made of copper material, and the middle layer is comprised of flame retardant (FR)-4 material, whose permittivity is 4.3 and height is 0.8 mm. The basic circular monopole antenna dimensions are approximated using the formulas given in [26] and [27]. The lower frequency (f_L) of the basic monopole antenna, relating to VSWR ≤2 is

$$f_L = \frac{7.2}{(L + r + w) \times k}\,(GHz), \tag{1}$$

where $r = 1.06$ mm is the effective radius of the circular-shaped patch, $L = 4.24$ mm is the diameter of the cylindrical-shaped monopole, $w = 0.52$ mm is the distance between the feed line with respect to the ground, and k is the empirical value of the FR-4 dielectric layer. The basic monopole antenna is comprised of a planar microstrip circular patch coupled to a microstrip feed line, as shown in Figure 2(a). To achieve the desired frequency band, the pattern of the radiating element is changed from the initial step of evolution to the final step. The basic circular monopole antenna generates a narrow operating band from 6.84 GHz to 7.37 GHz. Adjusting the distance between the patch and ground plane (w), modifying the electrical size of the patch, and changing the ground as structure help improve impedance matching, a wider bandwidth, and other performance metrics [28–30].To achieve the wider bandwidth with proper impedance matching, two elliptical-shaped radiators are integrated with the circular-shaped radiator, as shown in Figure 2(b). As a result, dual bands, from 3.7 GHz to 4.47 GHz and 5.98 GHz to 7.58 GHz, are obtained. In the third step of evolution, the circular radiator is further modified by adding two more elliptical-shaped radiators at 45° and 65°, respectively, on the left and right sides, as shown in Figure 2(c). As a result, the existing bands are shifted towards the lower frequency of the UWB. In Figure 2(d), semihexagonal-shaped slots and semicircular slots are introduced in the ground plane and radiator, respectively, to achieve a wider bandwidth from 3.14 GHz to 7.16 GHz. In Step 5, the ground plane is further modified by introducing rectangular and triangular-shaped slots, as illustrated in Figure 2(e). As a result, the desired ultra-wide band of 3.14 GHz to 11.17 GHz is achieved. Hence, the proposed UWM antenna resonates in the ultra-wide band with three resonating frequencies, 3.76 GHz, 6.7 GHz, and 9.8 GHz, with a reflection coefficient better than −20 dB.

The overall size of the final UWM antenna is $18 \times 19 \times 0.8$ mm^3. The designed parameters of the proposed UWM antenna are $L_{su} = 19$, $W_{su} = 18$, $R_0 = 1.48$, $R_1 = 6.89$, $R_2 = 3.2$, $R_3 = 2.2$, $R_4 = 5.6$, $R_5 = 2.5$, $R_6 = 6.3$, $R_7 = 2$, $Y_1 = 5.5$, $Y_2 = 1.5$, $Y_3 = 3.78$, $Y_4 = 1.46$, $Y_5 = 1.75$, and $Y_6 = 1.18$, and all dimensions are in mm. The schematic and fabricated prototypes of the proposed UWM antenna are shown in Figures 3(a) and 3(b), respectively. The S-parameter results from the evolution steps of the UWM antenna with a modified circular patch are shown in Figure 4. The fabricated antenna is measured using a Keysight Field Fox Microwave VNA (N9926A-14 GHz). The frequency response of the fabricated prototype ranges from 3.23 to 10.83 GHz. Figure 5 illustrates that across the entire ultra-wideband, the proposed UWM antenna has a realised gain of 2.1 to 3.86 dBi and a radiation efficiency ranging from 87.5 to 98.3%. And it is observed that the average radiation efficiency for the entire operating band is 92.3%, and the maximum gain is 3.91 dBi at 6.8 GHz.

In an anechoic chamber, the radiation performance of the proposed UWM antenna is measured. The normalized measured and simulated radiation patterns of the proposed UWM antenna for the $\varphi = 90°$ and $\varphi = 0°$ at the frequencies of 3.76, 6.7, and 9.8 GHz are plotted in Figure 6. The proposed UWM antenna has a stable omni-directional pattern for $\varphi = 0°$ and a bidirectional pattern for $\varphi = 90°$. The maximum measured gain of the proposed UWM antenna is 3.77 dBi at 5.97 GHz.

The frequency responses of the full-wave simulated and measured are presented in Figure 7 and appear to be quite similar. The comparative study between the proposed UWM antenna and other literature is depicted in Table 1. The proposed UWM antenna is more compact and has good isolation than the other reported works. It has a higher gain compared to the antennas in [31, 32]. It has a good average radiation efficiency when compared to the antennas in [33].

3. Results and Discussion

3.1. Investigation of SAR. In a full-wave simulator, a simple model of a tibia is designed using skin, fat, muscle, and bone in the shape of a cylinder, as shown in Figure 8. The tissue properties are assigned to a four-layer model according to the values given in [34, 35]. The radii of the layers are $b_1 = 15$ mm, $b_2 = 22.5$ mm, $b_3 = 30$ mm, and $b_4 = 30.4$ mm. The antenna is placed at a far-field distance of $F = 18$ mm from the surface of the skin. Also, to make it look like a broken bone, which is usually full of blood, a blood strip of length P mm (35, 25, etc.), width 10 mm, and height 5 mm is made between the bone and muscle, and at the bottom of the strip, a 6 mm-wide crack is created. First, we check the essential parameter, SAR, to make sure that the proposed UWM antenna works safely when it is close to a human body.

The input power (P_i) is set to 0 dBm, and the antenna is kept parallel to the surface of the tibia model without a crack at a far-field distance from the skin surface. As a result, the simulated SAR values are 0.015 (W/kg) (1 g) at 3.76 GHz, 0.025 (W/kg) (1 g) at 6.7 GHz, and 0.028 (W/kg) (1 g) at 9.8 GHz. To validate the IEEE standard public radiation exposure limit of 1.6 (W/kg) [36, 37], the input power is gradually increased from 0 to 18 dBm in various orders and plotted in Figure 9.

Therefore, the proposed UWM antenna with an input power of 18 dBm generates a SAR value of 1.239 (W/kg) (1 g) at 3.76 GHz, 1.541 (W/kg) (1 g) at 6.7 GHz, and 1.583 (W/kg)

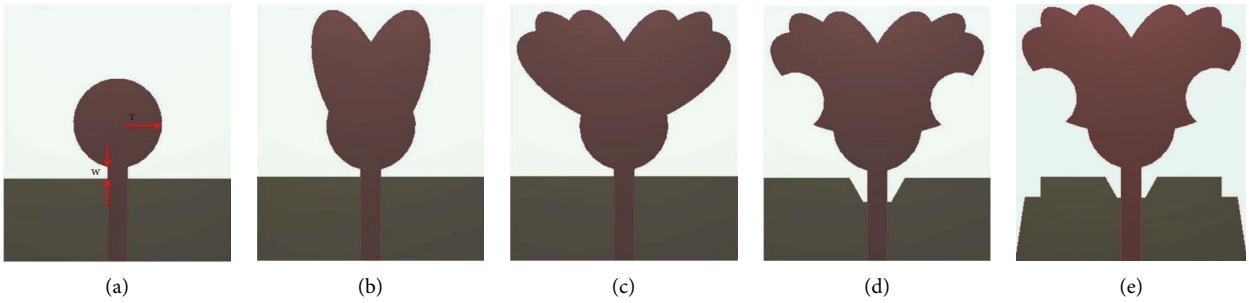

Figure 2: The design evolution of the proposed UWM antenna. (a) Step-1. (b) Step-2. (c) Step-3. (d) Step-4. (e) Proposed.

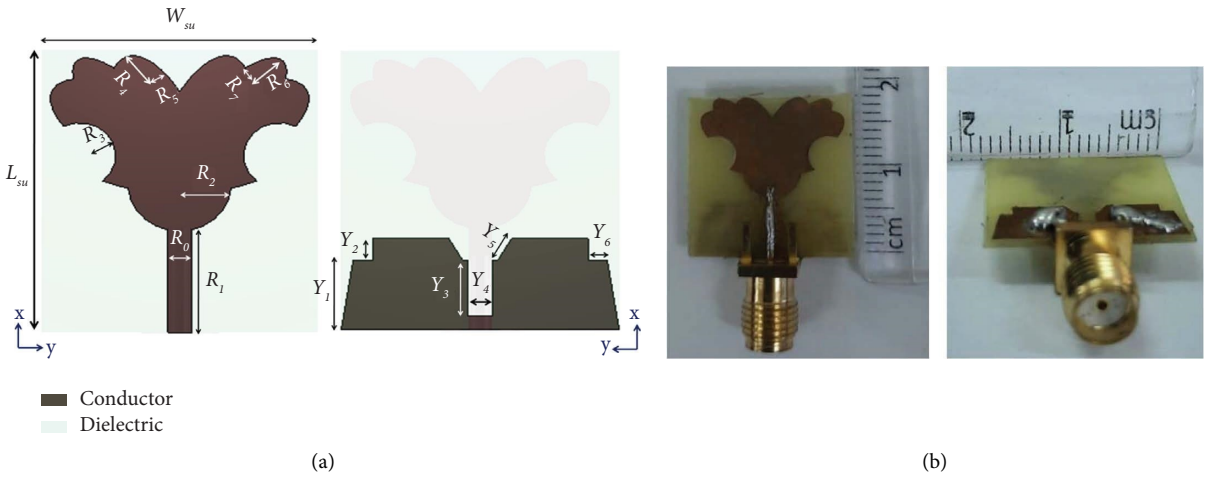

Figure 3: The top and bottom sides of the (a) designed and (b) fabricated prototype of the proposed UWM antenna.

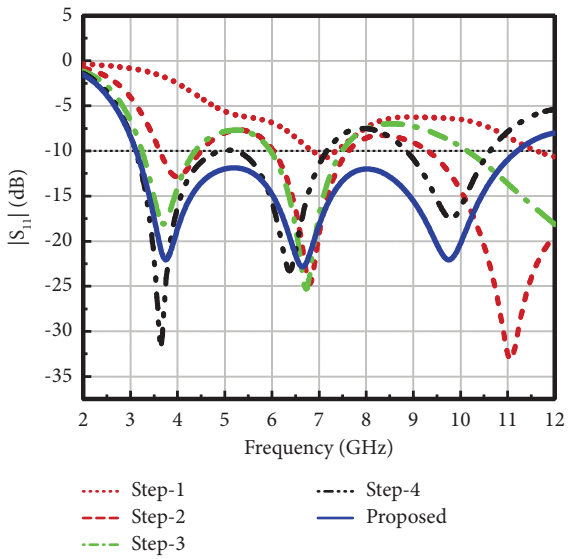

Figure 4: Frequency responses of the proposed UWM antenna evolution stages.

(1 g) at 9.8 GHz. Hence, the proposed UWM antenna achieves safe radiation exposure to the human body with $P_i = 18$ dBm and it will help to allow for deeper tissue penetration for better clinical responses [9].

3.2. Experimental Validation with Bovine Tibia. The layer of bovine skin and cortical bone is used to replicate a human leg in the experimental evaluation. Regarding electrical characteristics, bovine tissues are similar to human tissues

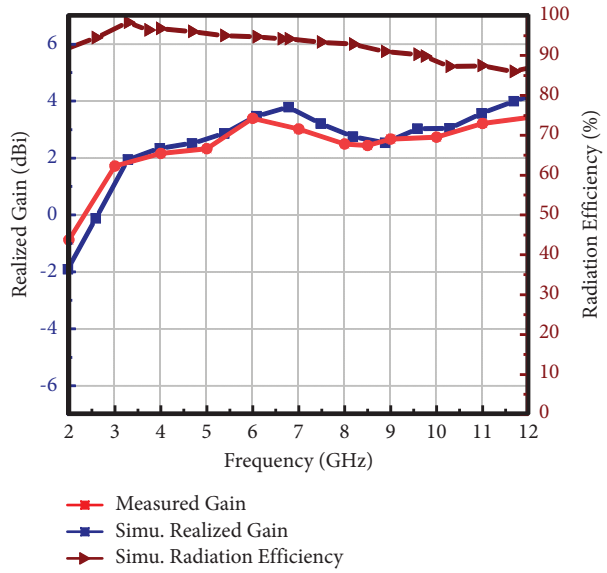

Figure 5: Radiation efficiency and gain of the proposed UWM antenna.

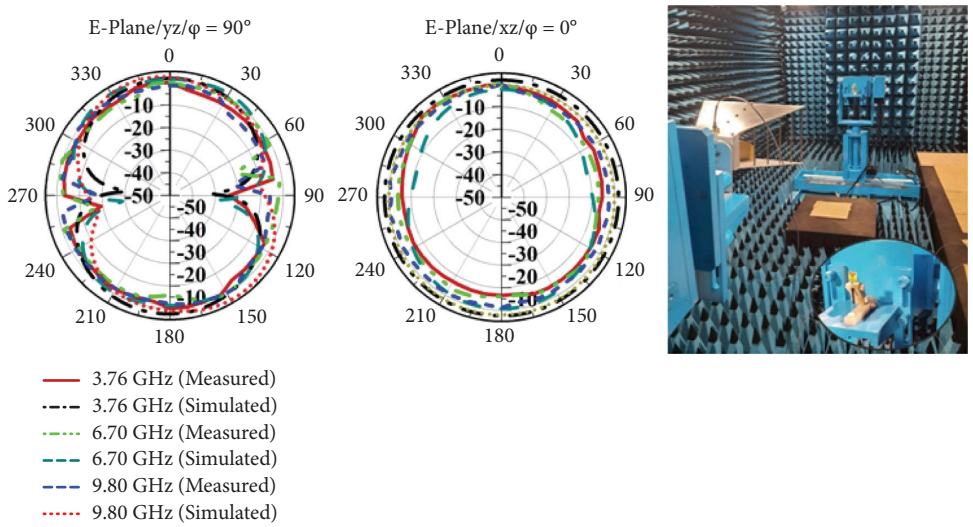

Figure 6: The radiation pattern of the UWM antenna for the $\varphi = 90^{\circ}$ and $\varphi = 0^{\circ}$.

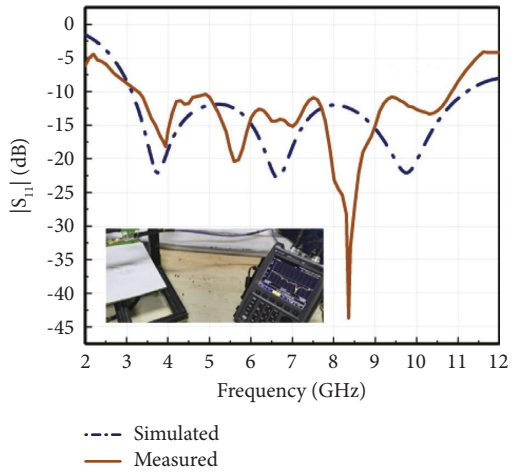

Figure 7: Full-wave simulated and measured $|S_{11}|$-parameters of the proposed UWM antenna.

Table 1: Comparative analysis among ultra-wideband monopole antennas of FR-4 substrate for biomedical applications and air as a medium.

References	$\lambda_0 \times \lambda_0$ (m^2)	Substrate thickness (mm)	Operating band (GHz)	Fractional bandwidth (%)	Avg. radiation efficiency (%) (simulated)	Max. realized gain (dBi)
[18]	0.270×0.290	1.6	3–15	133.33	—	—
[31]	0.238×0.330	1.6	3.1–12	117.88	—	3.54
[32]	0.157×0.217	1.6	2.95–12	121	—	3.6
[33]	0.207×0.310	1.6	3.1–6.8	105.71	89.2	6.8
Proposed	0.194×0.205	0.8	3.23–10.83	112.23	92.3	3.77

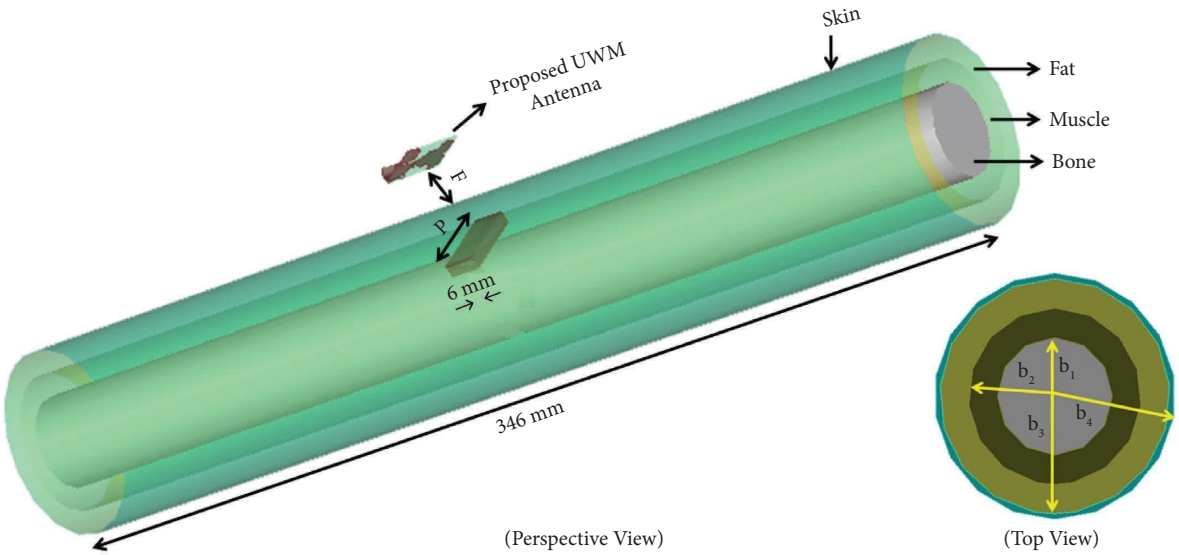

Figure 8: The tibia model in a full-wave simulator with the proposed UWM antenna.

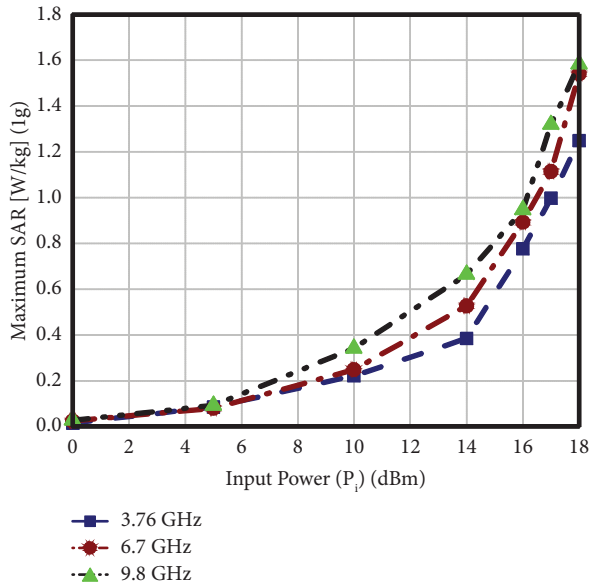

Figure 9: The plot for SAR values with respect to different values of input power.

[38, 39]. The schematic of the experimental setup is depicted in Figure 10. The bovine limb is positioned in front of the proposed antenna at a far-field distance. The system includes a vector network analyzer (VNA), a microcontroller with a stepper-motor-based sliding plate, a personal computer with MATLAB software, and an Android application. On

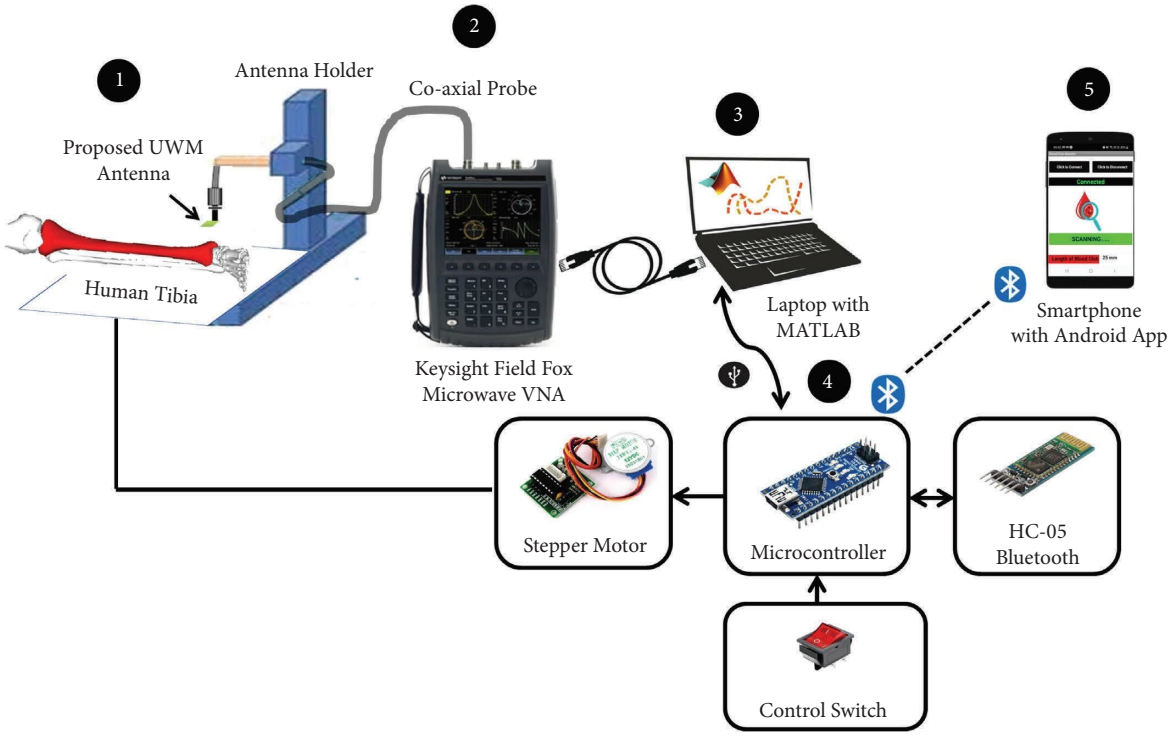

Figure 10: The schematic of the experimental setup to detect bone fracture and its recovery process.

the sliding platform, a pole with an antenna is mounted. The mechanically moving platform is capable of forward and reverse motion. The keysight field fox microwave VNA functions as a transceiver that transmits electromagnetic signals via the transmitting antenna [40]. This VNA is also connected to the computer through a general purpose interface bus (GPIB) port, which analyses the received data using MATLAB. And finally, the microcontroller with a wireless communication module is used to monitor the data in an Android application.

3.2.1. Fracture Detection. The experimental investigation is carried out on 6 mm-cracked and normal areas of the bovine tibia. The $|S_{11}|$-parameters for fractured and normal regions are recorded with 1001 frequency points and are plotted in Figure 11(a). A machine learning method, PCA, is applied to the recorded S-parameters. The PCA is a statistical unsupervised machine learning technique that translates multidimensional data into two principal components (PCs), which lie on the X and Y axis and are represented by PC-1 and PC-2.

PCA transforms data with m columns (features) into a subspace with m or less columns while preserving the original data's essence. In our application, the data set was interpreted as the reflection coefficients for 1001 frequency points in a normal area (N_A) and a fracture area (F_A). Therefore, the N_A and F_A datasets are represented as the two observations and detecting a fracture is accomplished by tracing the two coordinates representing the two spots in the 1001-dimensional data. If there is any correlation between the observations (N_A and F_A data sets), the associated points are observed as *PC1* and *PC2* in two-dimensional space. The PCA technique code is developed in MATLAB. The PCA result of the reflected signals from fractured and non-fractured bovine tibia regions is plotted in Figure 11(b). By observing the PCA plot in Figure 11(b), it is simple to distinguish between fractured and normal areas with the principal components, A_F and A_N.

3.2.2. Fracture Healing Monitoring. The experimental investigation of the fracture recovery process of the bovine tibia is shown in Figure 12. The fractured portion of the bovine tibia is covered with blood clot strips measuring $35 \times 10 \times 5\ \text{mm}^3$, $25 \times 10 \times 5\ \text{mm}^3$, and $15 \times 10 \times 5\ \text{mm}^3$ (one after the other), and the corresponding reflection parameters and lower cut-off frequency shifts are recorded and compared in Figure 13 to determine the relationship between blood-clot length and frequency shift, as noted in Table 2.

The LRA is one of the most prominent modelling approaches because it can estimate the value of a response variable based on the predictor variable [41]. Using LRA, the relationship between the length of the blood clot and the frequency shift is formulated, and it is given as

$$L_b = \left(35.0933 - 0.0401 \times F_s - 0.001 \times F_s^2\right) \pm \Delta E, \quad (2)$$

whereas the length of the blood clot (L_b) is the response variable, the frequency shift (F_s) is the predictor variable, and the error to best fit the response value, L_b, is $\Delta E = 0.517$. The average percentage of error calculated for the three predictor variables is less than 1%, and the goodness of fit (R square) is 0.935. Hence, the percentage of error is very low for the different lengths of blood clots. Therefore, equation (2) is

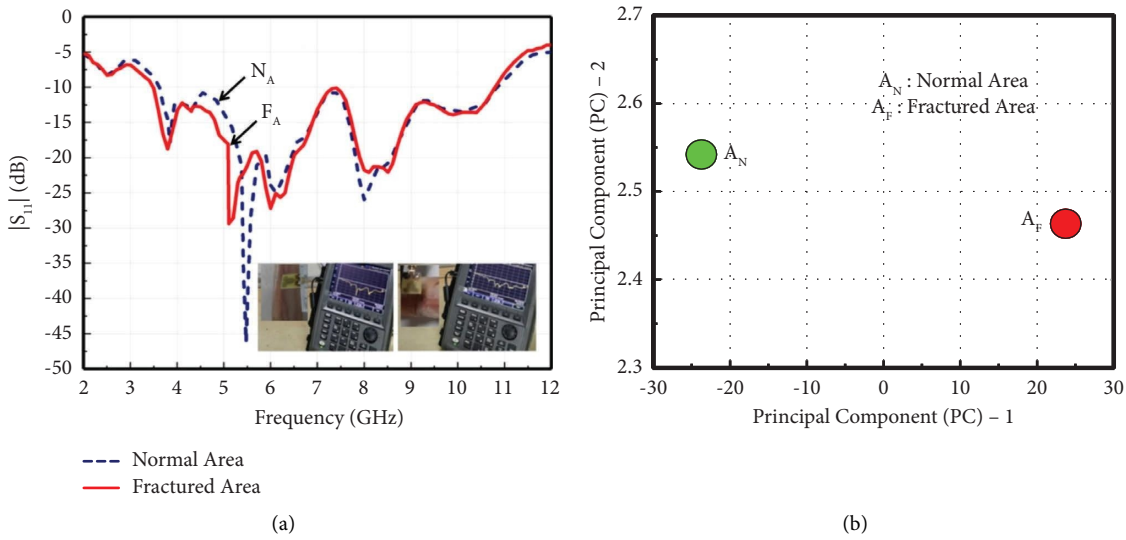

Figure 11: (a) The $|S_{11}|$-parameters and (b) PCA results for fracture and normal regions of the bovine tibia.

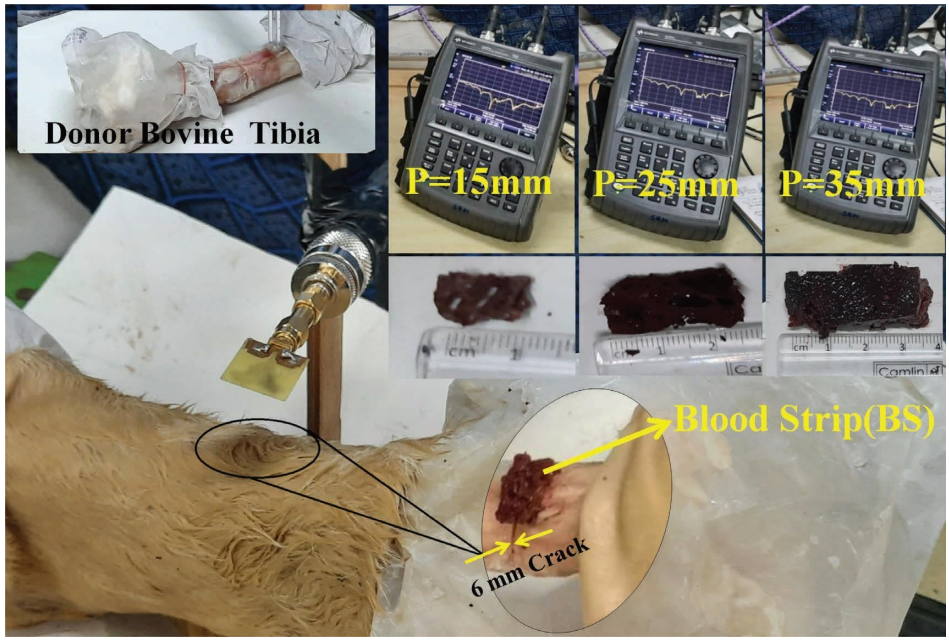

Figure 12: The experimental investigation of the fracture recovery process of the bovine tibia.

more accurate to measure the L_b for monitoring the fracture healing process.

An Android application for blood clot monitoring has been developed to measure the length of blood clots on mobile devices, and it is named blood clot monitor (BCM). The BCM application will connect wirelessly with a nearby microcontroller connected to the HC-05 Bluetooth module. The steps to create a wireless connection in the developed BCM application are as follows:

(1) Initializing the default Bluetooth device on an Android phone.

(2) Checking whether the HC-05 Bluetooth module's MAC address is connected to the microcontroller.

(3) A separate thread is created in the code to initiate a connection using the MAC address, and this thread will manage what happens if a link is successfully established or fails.

(4) Once a connection is established, the thread will call back for the codes that manage data exchange between two devices.

This thread will read the incoming data transmission from the microcontroller which is connected to the VNA through a graphical user interface, and the data are sent to the BCM application. The BCM application enables the user or physician to determine the status of fracture healing. Equation (2) is used in microcontroller programming to

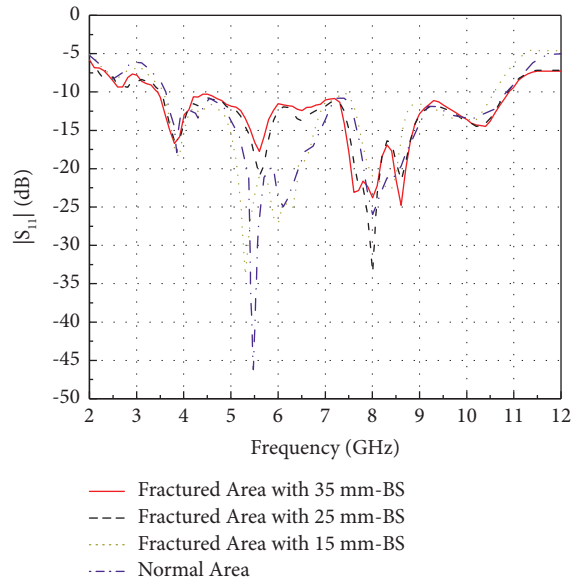

Figure 13: The $|S_{11}|$-parameters for blood clot strips of lengths 35 mm, 25 mm, and 15 mm and normal tibia.

Table 2: The lower cut-off frequency shift with respect to the blood clot strip lengths.

Blood clot strip length (P) (in mm)	Shifted frequency (F_s) (in MHz)
35	—
25	86
15	121
Normal tibia (without blood strip and fracture)	170

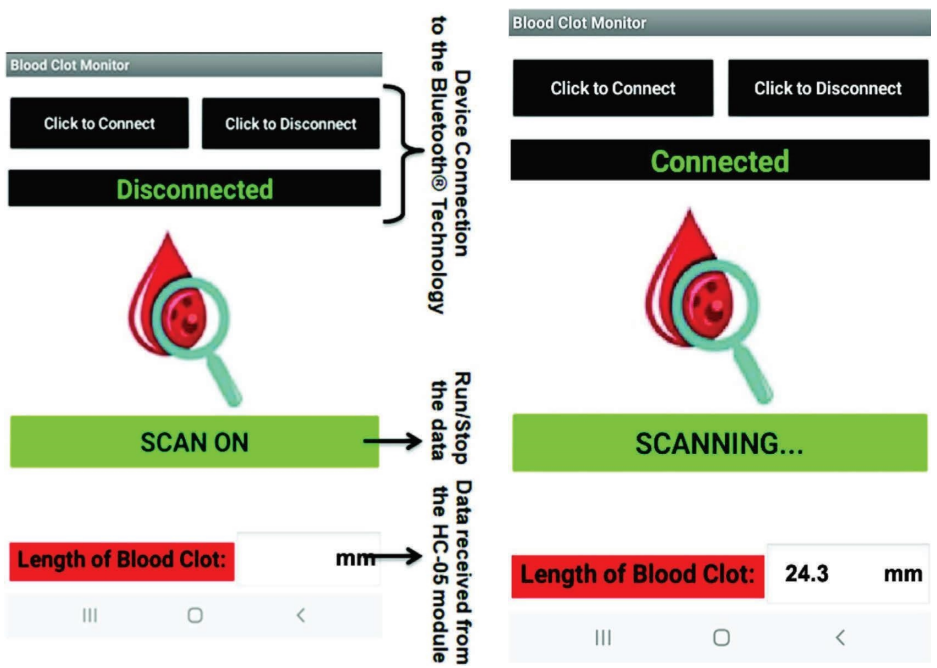

(a) (b)

Figure 14: The blood clots monitor application (a) before and (b) after scanning.

Table 3: Comparison of our investigation of bone fractures with other studies.

References	Objectives	Configurations	Operating frequency (GHz)	Phantom	Medium	Detection method	Portable system validation
[8]	Detecting transversal bone fractures	A planar microstrip sensor (S_{11} and S_{21} parameters)	2.45	A realistic porcine tibia bone	Contact with the body	Microwave imaging	No
[10]	Bone crack/void detection	A single planar monopole antenna (S_{11} parameters)	2.45	A realistic phantom of porcine tissues	Contact with the body	Frequency shifting	No
[42]	Reconstruction of bone profiles	An antipodal Vivaldi antennas (S_{11} and S_{21} parameters)	0.5–4	Fabricated bovine tibia	Contact with the body	Microwave imaging	No
[43]	Human bone health evaluation	A planar monopole antenna	3–7	No experimental validation	Contactless with the body	Time domain analysis	No
[44]	Detecting transversal bone fractures	A single antipodal Vivaldi antenna (S_{11} parameters)	8.3–11.1	A realistic phantom compose of animal tibia with skin	Contactless with the body	Microwave imaging	No
This work	Detection of bone fractures and their healing process	A single planar monopole antenna (S_{11} parameters)	3.23–10.83	3-layered real bovine tibia	Contactless with the body	Frequency shifting and machine learning	Yes (embedded system with Android application)

predict the length of a blood clot based on the frequency variation obtained from the proposed UWM antenna using MATLAB. Through the process of comparing the data points in MATLAB, the shifted frequency is transmitted to the serial port of the microcontroller. The mobile app is developed using an open-source web app builder. Figure 14(a) depicts the user interface of the developed application. The user interface consists of two layouts: the upper layout is for wireless connection and status, and the lower layout is for reading data from the HC-05 Bluetooth module.

When the user clicks on the "click to connect" button, the application shows the available Bluetooth networks in the surrounding area. The corresponding network should be selected, and the status of the connection is displayed on the below widget. After successful connection, user has to click on the "SCAN ON" button, and the data (blood clot length) is read from the HC-05 module via Bluetooth Technology and displayed on the respective widget, as shown in Figure 14(b). The comparison of this work on bone fracture healing with other studies is tabulated in Table 3.

The highlights of the proposed work are as follows:

(i) A compact planar monopole antenna is used in a noninvasive, nonionized method to identify bone fractures and monitor their recovery.

(ii) The proposed UWM antenna prototype is tested on bovine bone, and the effect of various lengths of blood clots along with fracture is analysed.

(iii) The approach based on machine learning is used on reflection coefficient parameters to detect fractures and their healing.

(iv) The proposed UWM antenna is integrated into the embedded hardware system.

(v) A new Android application is developed to access the data from the embedded hardware system.

(vi) The length of blood clots measured by the Android application and the recovery rate can be estimated by the user.

(vii) In comparison to previously reported works, the proposed diagnostic system has several advantages, including a noninvasive, precision, portability, the absence of a skilled technician, and a planar antenna (easy to integrate with RF/IoT devices) for crack detection and healing monitoring, which is relatively new.

4. Conclusion

A planar, 0.8-mm-thick ultra-wideband monopole antenna is designed and fabricated to monitor the fracture recovery process. The proposed UWM antenna has a maximum measured gain of 3.77 dBi and a simulated average radiation efficiency of 92.3% across the entire operating band. The tibia model is created in the full-wave simulator to analyse the SAR for various input power levels, and the resultant SAR values are below 1.6 (W/kg) (1 g) at input power of 18 dBm. The experimental study is also conducted on the bovine tibia and PCA and LRA is employed to detect and monitor the fracture recovery process, respectively. An embedded system-based setup with an Android application has been developed to monitor the healing status further. The experimental study has confirmed that it is possible to use a single antenna to monitor the stages of the recovery of a bone fracture for clinical diagnosis.

Data Availability

The data used to support the findings are available from the corresponding author upon request.

Conflicts of Interest

The authors declare that they have no conflicts of interest.

References

[1] Y. Du, W. Wang, and L. Wang, "Hierarchical recurrent neural network for skeleton based action recognition," in *Proceedings of the IEEE Conference on Computer Vision and Pattern Recognition*, pp. 1110–1118, Boston, MA, USA, June 2015.

[2] J. Kenwright, J. Richardson, J. Cunningham et al., "Axial movement and tibial fractures. a controlled randomised trial of treatment," *Journal of Bone and Joint Surgery British Volume*, vol. 73, no. 4, pp. 654–659, 1991.

[3] P. Villa and E. Mahieu, "Breakage patterns of human long bones," *Journal of Human Evolution*, vol. 21, no. 1, pp. 27–48, 1991.

[4] P. Raghavan and E. Christofides, "Role of teriparatide in accelerating metatarsal stress fracture healing: a case series and review of literature," *Clinical Medicine Insights: Endocrinology and Diabetes*, vol. 5, p. CMED.S9663, 2012.

[5] P. Elsissy, Y. T. Akpolat, A. Chien, and W. K. Cheng, "MRI evaluation of the knee with non-ferromagnetic external fixators: cadaveric knee model," *European Journal of Orthopaedic Surgery and Traumatology*, vol. 25, no. 5, pp. 933–939, 2015.

[6] M. Khan, S. P. S. M. A. Sirdeshmukh, and K. Javed, "Evaluation of bone fracture in animal model using bio-electrical impedance analysis," *Perspectives in Science*, vol. 8, pp. 567–569, 2016.

[7] M. Matsuda, M. Mizumoto, H. Kohzuki, N. Sugii, H. Sakurai, and E. Ishikawa, "High-dose proton beam therapy versus conventional fractionated radiation therapy for newly diagnosed glioblastoma: a propensity score matching analysis," *Radiation Oncology*, vol. 18, no. 1, pp. 1–7, 2023.

[8] V. S. Ramalingam, M. Kanagasabai, and E. F. Sundarsingh, "A compact microwave device for fracture diagnosis of the human tibia," *IEEE Transactions on Components, Packaging, and Manufacturing Technology*, vol. 9, no. 4, pp. 661–668, 2019.

[9] X. Lin, Y. Chen, Z. Gong, B.-C. Seet, L. Huang, and Y. Lu, "Ultra-wideband textile antenna for wearable microwave

medical imaging applications," *IEEE Transactions on Antennas and Propagation*, vol. 68, no. 6, pp. 4238–4249, 2020.

[10] A. V. Boologam, K. Krishnan, S. K. Palaniswamy et al., "On the design and development of planar monopole antenna for bone crack/void detection," *International Journal of Antennas and Propagation*, vol. 2022, pp. 1–12, 2022.

[11] M. C. Lin, D. Hu, M. Marmor, S. T. Herfat, C. S. Bahney, and M. M. Maharbiz, "Smart bone plates can monitor fracture healing," *Scientific Reports*, vol. 9, no. 1, p. 2122, 2019.

[12] K. Gupta, P. Gupta, G. Singh, S. Kumar, R. K. Singh, and R. Srivastava, "Changes in electrical properties of bones as a diagnostic tool for measurement of fracture healing," *Hard Tissue*, vol. 2, no. 1, p. 3, 2013.

[13] S. Symeonidis, W. G. Whittow, M. Zecca, and C. Panagamuwa, "Bone fracture monitoring using implanted antennas in the radius, tibia and phalange heterogeneous bone phantoms," *Biomedical Physics & Engineering Express*, vol. 4, no. 4, Article ID 045006, 2018.

[14] K. M. Labus, C. Sutherland, B. M. Notaros et al., "Direct electromagnetic coupling for non-invasive measurements of stability in simulated fracture healing," *Journal of Orthopaedic Research*, vol. 37, no. 5, pp. 1164–1171, 2019.

[15] V. Akdoğan, V. Özkaner, F. O. Alkurt, and M. Karaaslan, "Theoretical and experimental sensing of bone healing by microwave approach," *International Journal of Imaging Systems and Technology*, vol. 32, no. 6, pp. 2255–2261, 2022.

[16] A. Rula, "Patch antenna based on spiral split rings for bone implants," *Przeglad Elektrotechniczny*, vol. 7, pp. 129–134, 2020.

[17] M. Alibakhshikenari, B. S. Virdee, P. Shukla et al., "Metamaterial-inspired antenna array for application in microwave breast imaging systems for tumor detection," *IEEE Access*, vol. 8, pp. 174667–174678, 2020.

[18] S. Subramanian, B. Sundarambal, and D. Nirmal, "Investigation on simulation-based specific absorption rate in ultra-wideband antenna for breast cancer detection," *IEEE Sensors Journal*, vol. 18, no. 24, pp. 10002–10010 009, 2018.

[19] Y. Cheng and M. Fu, "Dielectric properties for non-invasive detection of normal, benign, and malignant breast tissues using microwave theories," *Thoracic cancer*, vol. 9, no. 4, pp. 459–465, 2018.

[20] M. M. Soliman, M. E. Chowdhury, A. Khandakar et al., "Review on medical implantable antenna technology and imminent research challenges," *Sensors*, vol. 21, no. 9, p. 3163, 2021.

[21] S. Ashok Kumar and T. Shanmuganantham, "Design of clover slot antenna for biomedical applications," *Alexandria Engineering Journal*, vol. 56, no. 3, pp. 313–317, 2017.

[22] A. F. Mirza, C. H. See, I. M. Danjuma et al., "An active microwave sensor for near field imaging," *IEEE Sensors Journal*, vol. 17, no. 9, pp. 2749–2757, 2017.

[23] M. Alibakhshi-Kenari, M. Naser-Moghadasi, and R. Sadeghzadeh, "The resonating MTM-based miniaturized antennas for wide-band RF-Microwave systems," *Microwave and Optical Technology Letters*, vol. 57, no. 10, pp. 2339–2344, 2015.

[24] A. H. Naghavi, H. R. Hassani, and D. Oloumi, "Investigation and analysis of em pulse propagation inside human head for high-resolution UWB elliptical SAR imaging," *IEEE Journal of Electromagnetics, RF and Microwaves in Medicine and Biology*, vol. 6, no. 4, pp. 485–493, 2022.

[25] J. Lever, M. Krzywinski, and N. Altman, "Points of significance: principal component analysis," *Nature Methods*, vol. 14, no. 7, pp. 641-642, 2017.

[26] N. P. Agrawall, G. Kumar, and K. Ray, "Wide-band planar monopole antennas," *IEEE Transactions on Antennas and Propagation*, vol. 46, no. 2, pp. 294-295, 1998.

[27] K. Ray and Y. Ranga, "Ultra-wideband printed elliptical monopole antennas," *IEEE Transactions on Antennas and Propagation*, vol. 55, no. 4, pp. 1189–1192, 2007.

[28] S. Doddipalli, A. Kothari, and P. Peshwe, "A low profile ultrawide band monopole antenna for wearable applications," *International Journal of Antennas and Propagation*, vol. 2017, pp. 1–9, 2017.

[29] M. Kenari and M. Moghadasi, "UWB miniature antenna based on the CRLH-TL with increase gain for electromagnetic requirements," *Advanced Electromagnetics*, vol. 3, no. 1, pp. 61–65, 2014.

[30] H. T. Sediq, J. Nourinia, C. Ghobadi, and B. Mohammadi, "A novel shaped ultrawideband fractal antenna for medical purposes," *Biomedical Signal Processing and Control*, vol. 80, Article ID 104363, 2023.

[31] M. Islam, M. Islam, M. Samsuzzaman, M. Faruque, and N. Misran, "Microstrip line-fed fractal antenna with a high fidelity factor for UWB imaging applications," *Microwave and Optical Technology Letters*, vol. 57, no. 11, pp. 2580–2585, 2015.

[32] Z. Lasemi and Z. Atlasbaf, "Impact of fidelity factor on breast cancer detection," *IEEE Antennas and Wireless Propagation Letters*, vol. 19, no. 10, pp. 1649–1653, 2020.

[33] P. K. Rao and R. Mishra, "Resonator based antenna sensor for breast cancer detection," *Progress in Electromagnetics Research M*, vol. 101, pp. 149–159, 2021.

[34] C. Gabriel, *Compilation of the Dielectric Properties of Body Tissues at RF and Microwave Frequencies*, Defense Technical Information Center, Fort Belvoir, VA, USA, 1996.

[35] B. Amin, A. Shahzad, D. Kelly, M. O'Halloran, and M. Adnan Elahi, "Anthropomorphic calcaneus phantom for microwave bone imaging applications," *IEEE Journal of Electromagnetics, RF and Microwaves in Medicine and Biology*, vol. 5, no. 3, pp. 206–213, 2021.

[36] International Commission on Non-Ionizing Radiation Protection ICNIRP, "Guidelines for limiting exposure to time-varying electric, magnetic, and electromagnetic fields (up to 300 GHz). International Commission on Non-Ionizing Radiation Protection," *Health Physics*, vol. 74, no. 4, pp. 494–522, 1998.

[37] The Institute of Electrical and Electronics Engineers Inc, *IEEE Standard for Safety Levels with Respect to Human Exposure to Electric, Magnetic, and Electromagnetic fields, 0Hz to 300 GHz*, IEEE, Manhattan, NY, USA, 2019.

[38] B. Amin, M. A. Elahi, A. Shahzad, E. Porter, B. McDermott, and M. O'Halloran, "Dielectric properties of bones for the monitoring of osteoporosis," *Medical, & Biological Engineering & Computing*, vol. 57, no. 1, pp. 1–13, 2019.

[39] B. Amin, A. Shahzad, L. Farina et al., "Dielectric characterization of diseased human trabecular bones at microwave frequency," *Medical Engineering and Physics*, vol. 78, pp. 21–28, 2020.

[40] M. Islam, M. Mahmud, M. T. Islam, S. Kibria, and M. Samsuzzaman, "A low cost and portable microwave imaging system for breast tumor detection using uwb directional antenna array," *Scientific Reports*, vol. 9, no. 1, p. 15491, 2019.

[41] R. Prasanna, K. Annaram, and K. Venkatalakshmi, "Early detection of acute coronary syndrome through prothrombin time measurement using flexible UWB antenna for cardiac patient," *Biomedical Signal Processing and Control*, vol. 76, Article ID 103636, 2022.

[42] G. Ruvio, A. Cuccaro, R. Solimene, A. Brancaccio, B. Basile, and M. J. Ammann, "Microwave bone imaging: a preliminary scanning system for proof-of-concept," *Healthcare technology letters*, vol. 3, no. 3, pp. 218–221, 2016.

[43] S. Ruchi Kerketta and D. Ghosh, "Microwave sensing for human bone health evaluation," *AEU-International Journal of Electronics and Communications*, vol. 127, Article ID 153469, 2020.

[44] K. C. Santos, C. A. Fernandes, and J. R. Costa, "Feasibility of bone fracture detection using microwave imaging," *IEEE Open Journal of Antennas and Propagation*, vol. 3, pp. 836–847, 2022.